Identifying Laguerre-Gaussian Modes using Convolutional Neural Network

Safura Sharifi^{1,2,3}, Yaser Banadaki^{3,4}, Elisha Siddiqui³, Savannah Cuzzo⁵, Narayan Bhusal³, Lior Cohen³, Austin Kalasky⁵, Nik Prajapati⁵, Rachel Soto-Garcia³, Sofia Brown⁵, Irina Novikova⁵, Eugeniy Mikhailov⁵, Georgios Veronis^{1,2}, Jonathan Dowling³

¹School of Electrical Engineering & Computer Science,

²Center for Computation and Technology,

³Hearne Institute for Theoretical Physics, Department of Physics and Astronomy,

Louisiana State University, Baton Rouge, Louisiana 70803, USA

Email: yaser_banadaki@subr.edu

Department of Physics, College of William and Marry, Williamburg, Virginia, 8795, USA
Emails: {slcuozzo, atkalasky, nprajapati, scbrown01, inovikova, eemikh}@email.wm.edu

Abstract— An automated determination of Laguerre-Gaussian (LG) modes benefits cavity tuning and optical communication. In this paper, we employ machine learning techniques to automatically detect the lowest sixteen LG modes of a laser beam. Convolutional neural networks (CNN) are trained by collecting the experimental and simulated datasets of LG modes that relies only on the intensity images of their unique patterns. We demonstrate that the trained CNN model can detect LG modes with the maximum accuracy greater than 96% after 60 epochs. The study evaluates the CNN's ability to generalize to new data and adapt to experimental conditions.

Keywords— Convolutional neural networks, Laguerre-Gaussian modes, cavity tuning, optical communication

I. INTRODUCTION

Laser beam profiling is necessary for most laser applications ranging from optical communications [1] to atomic physics [2]. Orbital angular momentum (OAM) beams allow for increased channel capacity in free-space optical communication. However, Laguerre-Gaussian (LG) modes are prone to mode loss and mode cross-talk [3, 4]. Therefore, identifying the mode information using the scale factors such as centroid and radius of a beam profile captured by a CCD or CMOS camera is challenging [5]. Recently, convolutional neural networks (CNNs) [6] and transfer learning approach [7] have been shown to remarkably improve the automated image interpretation with near human accuracy [8]. The technique has recently been applied to the related task of detecting OAM modes [9] with accuracies far better than those of the conjugate-mode sorting method [10]. Hofer et al. [11] used a CNN to accurately determine the Hermite-Gaussian (HG) mode of a laser beam. Lohani et al. [1] demonstrated the ability of deep neural networks to classify LG modes when the training and test datasets are generated using computer simulation.

In this paper, we employ a CNN to automatically classify the LG modes based on only the intensity profile of their unique patterns obtained using two experimental setups and simulated data. The intensity profile of the detected modes allows for considerable simplification of current measurement schemes and potentially results in lower error rates than the scale factors techniques. The substantial amount of labeled simulation and experimental datasets were generated for the training, validation, and testing in order to strengthen the CNN's ability to generalize and adapt to experimental conditions. Gaussian noise, Poisson noise, speckle noise, and camera blur are added to the simulated images in MATLAB to replicate imperfections of real experimental conditions. In order to train the CNN architecture for interpreting and classifying the LG modes, we re-train the Inception-v3 [12] model of the TensorFlow platform [13], Google's deep learning open source software. We demonstrate that the trained CNN model using the theoretical and experimental datasets can generalize to new data with the maximum accuracy of >96% after 60 epochs. However, the CNN model trained by the simulated images cannot effectively adapt to the experimental data, so that its accuracy is evaluated to be ~70% and ~50% for the first and second experiments, respectively.

The paper is organized as follows: Section II presents the theoretical framework of LG modes, and two experimental setups that are used to collect the training datasets, followed by a discussion of training procedure for a CNN model in Section III. In Section IV, we detail our results and assess the strengths and limits of the CNN model for automated identification of LG modes. Finally, Section IV summarizes our conclusions and the potential future directions of the work.

II. DATA COLLECTION OF LG MODES

A. Collecting Theoretical dataset

Gaussian-beam modes are the solutions of the free-space Maxwell's equations within the paraxial approximation called Laguerre-Gaussian (LG) modes in cylindrical coordinates and Hermite-Gaussian (HG) modes in Cartesian coordinates. The LG modes can be calculated by the theoretical expression below [14],

$$u_{l,p}(r,\phi,z) = \frac{C_{lp}^{LG}}{w(z)} \left(\frac{r\sqrt{2}}{w(z)}\right)^{|l|} \exp\left(-\frac{r^2}{w^2(z)}\right)$$

$$L_p^{|l|} \left(\frac{2r^2}{w^2(z)}\right) \exp\left(-ik\frac{r^2}{2R(z)}\right) \exp(-ikz)$$

$$\exp(il\phi) \exp\left[i(2p+|l|+1)\zeta(z)\right], \tag{1}$$

where r, φ and z are cylindrical coordinates; l and p are the azimuthal and radial indices, which are integers; p>0; $C_{lp}^{LG}=\sqrt{2\,p!/\pi\,(|l|+p)!}$ is a normalization constant; $L_p^{|l|}$ is the associated Laguerre polynomial; λ is the wavelength; $k=2\pi/\lambda$ is the wave number; $\omega(z)=\omega_0\sqrt{1+(z/z_R)^2}$ is the beam waist; ω_0 is the beam waist at the beam focus; $z_R=\pi\omega_0^2/\lambda$ is the Rayleigh range; $R(z)=z[1+(z/z_R)^2]$ is the radius of curvature; $\zeta(z)=\arctan(z/z_R)$ is the Gouy phase. Equation (1) is used to generate theoretical images dataset of the first 16 LG modes (1 and p vary from 0 to 3) for training the CNN model.

B. Collecting Experiemntal Dataset

The experimental data is generated using two experimental setups as follows:

1) First Experimental Setup

Figure 1 shows our first experimental setup that generates LG modes. The laser beam with the wavelength of 633 nm is coupled to a single mode fiber (SMF) before being collimated with the 5cm lens which helps us to clean the beam to a gaussian beam. The collimated gaussian beam hits the SLM (spatial light modulator) where desired LG modes are encoded holographically. The SLM is programmable and the projected light to the mask or hologram can be controlled through a computer program. The reflected beam from SLM contains many diffraction orders. We set our parameters such that the first diffraction order is bright enough to be used for the experiment. An iris placed at the Fourier plane acts as a filter to select the desired diffraction order. The beam profile thus selected is collimated with the final 25cm lens. A CCD camera at image plane records the intensity profiles of desired LG modes.

2) Second Experimental Setup

The second experimental setup for LG modes generation is depicted in Fig. 2. We use 795 nm laser that is coupled into a single-mode fiber and propagates through a telescope formed by two lenses to increase the size of the laser beam and illuminate as much SLM area as possible. The beam is pass through iris for additional mode cleaning, and then the wave plate and polarization beam splitter combo are used for controlling the light power, as well as for making sure the light polarization is

Identify applicable funding agency here. If none, delete this text box.

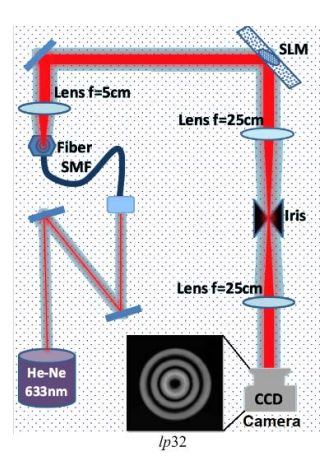


Fig.1. First experimental setup for generating arbitrary LG beams.

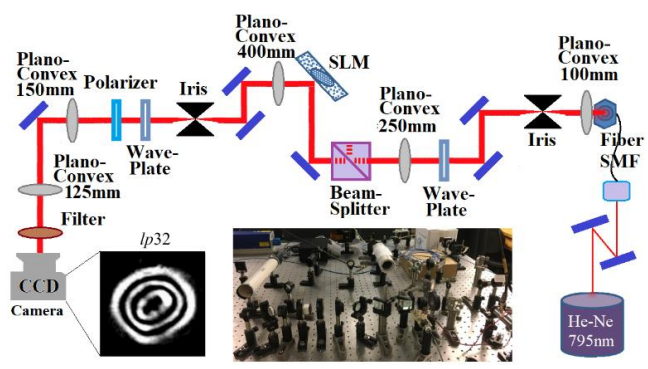


Fig.2. Second experimental setup for generating arbitrary LG beams.

correct at the SLM. The edge mirror reflects beam to SLM, and then a regular mirror picks up the reflected beam. The combination of three lenses after SLM is to focus the beam at the iris that cleans up any higher diffraction orders, shrink the beam back to small size and focus it on camera. In the second experimental setup, the light travels through more optical elements and lenses and thereby the quality of mode is lower than the first experimental setup. As such, this experiment data will diversify the training data with more spatial dislocation and non-uniform intensity in LG modes.

III. MACHINE LEARNING METHOD

A Convolutional Neural Networks within a deep learning framework uses multilayer convolution to extract features and combine the features automatically as shown in Fig. 3. The CNN extracts spatial features that are then passed to aggregation layers (averaging, pooling, etc.) and additional layers of filters for extracting higher-order features (patterns) that are combined at the top layer for LG mode interpretation and classification as shown in Fig.3. During the training steps, all the weights were obtained using forward- and backward- propagations through the CNN architecture.

We employ the CNN architecture and retrain the Inceptionv3 [12] model of the TensorFlow platform [13], Google's deep learning open source software, in interpreting and classifying the LG modes. TensorFlow has the advantages of high availability, high flexibility, and high efficiency. Transfer learning extracts existing knowledge learned from one environment to solve the other new problems such that the pretrained CNNs takes the advantage of training with a lower amount of data for the new problem and significantly shortened the training time. The labeled datasets were generated for training CNNs including a simulated dataset using Eq.(1) and an experimental dataset using the setups of a spatial light modulator (SLM) and beam profiler. To examine the CNN's ability to generalize to new data, two transforms were used during training. In the first transform, the training data is only selected from theory dataset whereas the second transform includes both theory and experiment datasets to increase the diversity of the CNN's training data.

The maximum amplitude of simulated modes is scaled to the experimental data by adjusting the contrast and beam waist at the beam focus. Gaussian noise, Poisson noise, speckle noise, and camera blur are also added to the simulated mode images to replicate imperfections of real experimental scenario. The standard deviations of the noises are randomly changed with a standard deviation of $\sigma = 0.02$. The training, validation, and test datasets consist of 200, 40, and 40 JPEG images (300×300 pixels) respectively for each of the LG modes, where p and l ranging from 0 to 3. For the optimization algorithm, we used stochastic gradient descent (SGD) with image batch size of 16 and learning rate equal to 0.01.

IV. RESULT AND DISCUSSION

Figure 4 shows the training and validation accuracy versus epoch (number of times the entire dataset is passed through the CNN) for two training datasets of only simulated images and both simulated and experimental images. It can be observed that training the CNN model with theory dataset reaches the maximum accuracy of 100% after 7 epochs while training with the second dataset that includes both theory and experiment images needs 33 epochs to reach the same maximum accuracy due to the diversity of the images. Similarly, the validation accuracy of 100% is achieved after 58 and 350 epochs for the two training datasets, one consisting of only the simulated images and the other containing both the simulated and experimental images, respectively. The inset table in Fig. 4 shows the accuracy of the CNN model on 10% test images of datasets at 6, 60, and 350 epochs. A maximum accuracy of 92% and 81.7% are achieved after 6 epochs on the simulated dataset and both simulated and experimental dataset, respectively. The values reach to 99.2% and 96.3% after 60 epochs.

Although the CNNs achieved high accuracy on test set of the simulated and experimental datasets, the model trained by the simulated images cannot fully generalize to experiment data, so that its accuracy is evaluated ~70% and ~50% for the first and second experimental setups, respectively. Figure 5 shows the prediction confidence on two LG modes (l=1, p=3 and l=1, p=1) obtained from the first experimental setup. For the CNN model that trained using the simulated images and tested on experiment data (dark red and dark blue), the LG mode of l=1, p=3 is correctly predicted in left graph with about 5 percent margin, however the LG mode of l=1, p=1 is incorrectly predicted as l=1, p=2 in the right graph. These prediction confidences are increased to 97% and 99% for the LG modes of l=1, p=3 and l=1, p=1, respectively, when the CNN models are trained using the both simulated and experiment data.

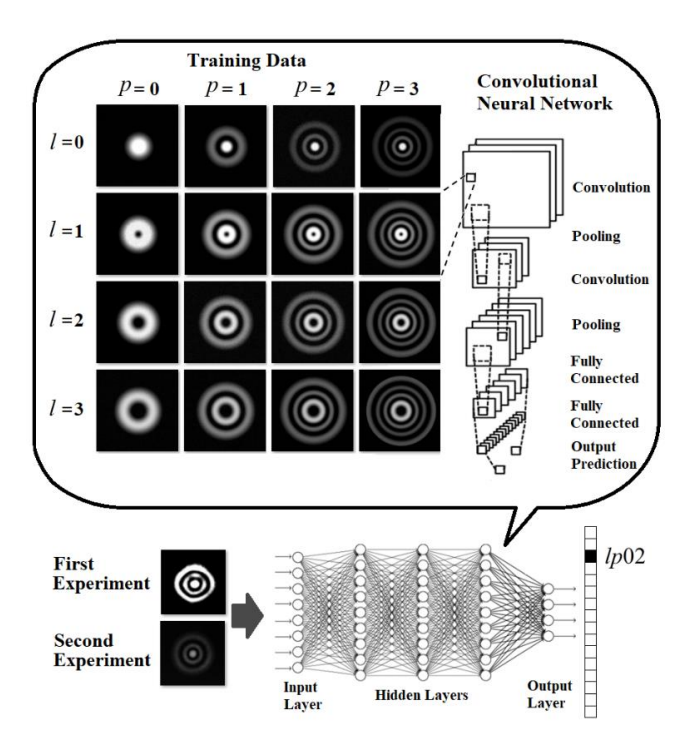


Fig.3. Training dataset of first 16 LG modes (1 and p vary from 0 to 3) are passed to the CNN model that extracts spatial features using aggregation layers (averaging, pooling, etc.) and additional filter layers that are eventually combined at the top layer to predict and classify the new image of LG mode.

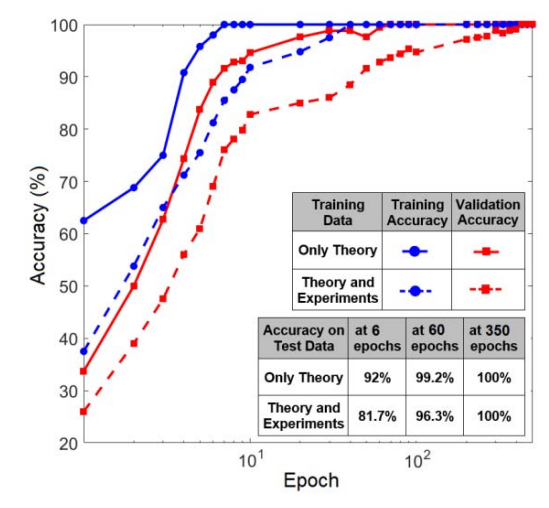


Fig.4. Training and validation accuracies versus epoch for two CNN models that are trained using the datasets of only simulated images (solid lines) and both simulated and experimental images (dashed lines). Inset table depicts the accuracy of the CNN models on 10% test images of the datasets at 6, 60, and 350 epochs.

Figure 6 shows the prediction confidence on two LG modes (l=0, p=1 and l=3, p=1) obtained from the second experimental setup. For the CNN model that trained using the simulated images and tested on experiment data (dark red and dark blue in left graph), the LG mode of l=0, p=1 is correctly predicted with the confidence of 88% and margin of ~85% from second and

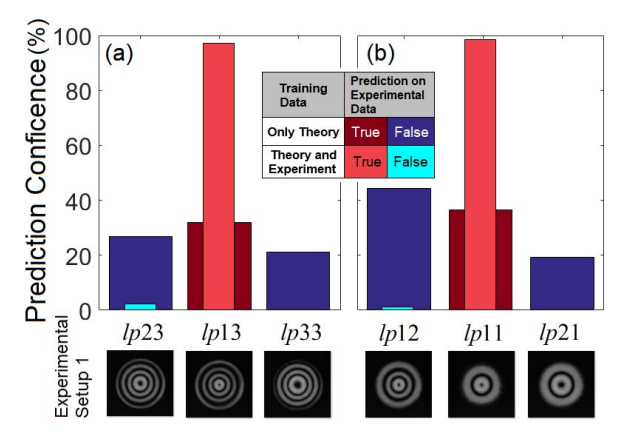


Fig. 5. Prediction confidence on two LG modes: (a) l=1, p=3 and (b) l=1, p=1 that are obtained from the first experimental setup. The dark red and dark blue indicate the results of the CNN models trained using the simulated images while the light red and light blue indicate the results of the CNN models trained using both the simulated and experiment images.

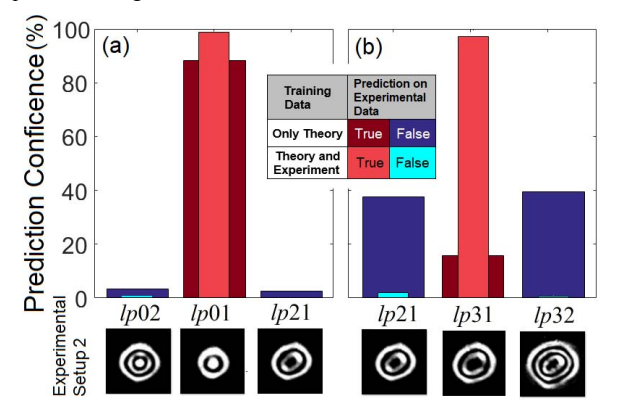


Fig. 6. Prediction confidence on two LG modes: (a) l=0, p=1 and (b) l=3, p=1 that are obtained from the second experimental setup. The dark red and dark blue indicate the results of the CNN models trained using the simulated images while the light red and light blue indicate the results of the CNN models trained using both the simulated and experiment images.

third possible mode (l=0, p=2). In the right graph, however, the LG mode of l=3, p=1 is incorrectly predicted as l=3, p=2 with prediction confidence of 38%. These prediction confidences are increased to 98.7% when the CNN model is trained using both the simulated and experimental data.

V. SUMMARY AND CONCLUSION

We have demonstrated that a convolution neural network can be used to automatically detect and classify the lowest sixteen unique Laguerre-Gaussian modes of a laser cavity. To effectively train the CNN, we prepared a large dataset consisting of both simulated and experimental images for each LG mode. The classification accuracy of 100% is achieved for the training dataset consisting of both simulated and experiment images of LG modes. However, the CNN trained only using the simulated data reaches to ~70% and ~50% accuracies for the first and

second experimental setups respectively. The difference is mainly due to the degree of imperfections like spatial dislocation and non-uniform illumination present in the experimental images of beam profiles.

The trained CNN model can be used to automatically detect LG modes in optical communications or tune the LG mode output of a laser cavity. This paper is only an initial exploration of this technique and further work needs to be done in preprocessing the theoretical data to comply with experimental data. This work contributes to determining the image data from the superpositions of various of OAM in a multiplexed beam without explicitly demultiplexing the beam with optics. An automated technique for demultiplexing of Hermite-Gaussian (HG) and Laguerre-Gaussian (LG) modes can enhance the information capacity of optical communication systems.

REFERENCES

- S. Lohani, E. M. Knutson, M. O'Donnell, S. D. Huver, and R. T. Glasser, "On the use of deep neural networks in optical communications," Applied optics, vol. 57, no. 15, pp. 4180-4190, 2018.
- [2] M. Clifford, J. Arlt, J. Courtial, and K. Dholakia, "High-order Laguerre– Gaussian laser modes for studies of cold atoms," Optics Communications, vol. 156, no. 4-6, pp. 300-306, 1998.
- [3] B. Ndagano, N. Mphuthi, G. Milione, and A. Forbes, "Comparing mode-crosstalk and mode-dependent loss of laterally displaced orbital angular momentum and Hermite–Gaussian modes for free-space optical communication," Optics letters, vol. 42, no. 20, pp. 4175-4178, 2017.
- [4] M. A. Cox, L. Maqondo, R. Kara, G. Milione, L. Cheng, and A. Forbes, "The resilience of Hermite-and Laguerre-Gaussian modes in turbulence," Journal of Lightwave Technology, vol. 37, no. 16, pp. 3911-17, 2019.
- [5] L. R. Hofer, R. V. Dragone, and A. D. MacGregor, "Scale factor correction for Gaussian beam truncation in second moment beam radius measurements," Optical Engineering, vol. 56, no. 4, p. 043110, 2017.
- [6] S. Hoo-Chang et al., "Deep convolutional neural networks for computeraided detection: CNN architectures, dataset characteristics and transfer learning," IEEE transactions on medical imaging, vol. 35, no. 5, p. 1285, 2016
- [7] A. Quattoni, M. Collins, and T. Darrell, "Transfer learning for image classification with sparse prototype representations," Proceedings of the IEEE conference on computer vision and pattern recognition (CVPR) 2008, pp. 1-8.
- [8] Y. Taigman, M. Yang, M. A. Ranzato, and L. Wolf, "Deepface: Closing the gap to human-level performance in face verification," Proceedings of the IEEE conference on computer vision and pattern recognition (CVPR), 2014, pp. 1701-1708.
- [9] T. Doster and A. T. Watnik, "Machine learning approach to OAM beam demultiplexing via convolutional neural networks," Applied optics, vol. 56, no. 12, pp. 3386-3396, 2017.
- [10] G. Gibson et al., "Free-space information transfer using light beams carrying orbital angular momentum," Optics express, vol. 12, no. 22, pp. 5448-5456, 2004.
- [11] L. Hofer, L. Jones, J. Goedert, and R. Dragone, "Hermite–Gaussian mode detection via convolution neural networks," JOSA A, vol. 36, no. 6, pp. 936-943, 2019.
- [12] C. Szegedy, V. Vanhoucke, S. Ioffe, J. Shlens, and Z. Wojna, "Rethinking the inception architecture for computer vision," Proceedings of the IEEE conference on computer vision and pattern recognition (CVPR), 2016, pp. 2818-2826.
- [13] M. Abadi et al., "Tensorflow: a system for large-scale machine learning," Operating Systems Design and Implementation (OSDI), 2016, vol. 16, pp. 265-283.
- [14] A. E. Siegman, "Lasers university science books," Mill Valley, CA, vol. 37, no. 208, p. 169, 1986.